Can UAVs fill the gap between *in situ* surveys and satellites for habitat mapping ?

Emilien Alvarez-Vanhard [1,3] *; Thomas Houet [1,3]; Cendrine Mony [2,3]; Lucie Lecoq [2,3]; Thomas Corpetti [1]

[1] CNRS UMR 6554 LETG, Université Rennes 2, Place du recteur Henri le Moal, 35000 Rennes, France

[2] CNRS UMR 6553 ECOBIO, Université Rennes 1, Avenue Général Leclerc, 35000 Rennes, France

[3] LTSER site “ZA Armorique”

* Corresponding author: alvarez_emilien@live.fr

Abstract:

Habitat mapping is an essential descriptor to monitor and manage natural or semi-natural ecosystems. Habitats integrate both the environmental conditions and the related biodiversity. However, it remains challenging to map certain habitats such as inland wetlands due to spectral, spatial and temporal variability in the vegetation cover. Currently, no satellite constellations optimize the spectral, spatial and temporal resolutions required to map wetlands according to the habitats discriminated from *in situ* surveys. Our approach aims to combine satellite and unmanned aerial vehicle (UAV) data to exceed their respective limitations. Both data sources were combined through a spectral unmixing algorithm with the hypothesis that endmembers from UAV data are pure enough to enhance plant community abundances estimated from satellite data. The experiment was conducted on the regional preserve of the Sougéal marsh, a wet grassland of 174 ha located upstream of the Mont-Saint-Michel Bay. Two satellite data sources - Sentinel-2 and Pleiades - and three acquisition periods - November 2017, April 2018 and May 2018 - were considered. A reference map of plant community distribution was produced from UAV multitemporal data and floristic surveys to validate the unmixing of satellite data. This study shows innovative results and perspectives: while UAV can improve habitat discrimination, results vary among acquisition periods and habitats. Results illustrate well the great potential of combined UAV and satellite data but also demonstratethe influence of endmembers on the unmixing process and technical limitations (e.g. spectral mismatches between sensors), which can be overcome using domain adaptation.

Keywords: Unmanned Aerial Vehicle; sensor synergy; endmember; wetlands; spectral unmixing; habitat mapping; LTSER Armorique

1. Introduction

Global changes caused by human activities are a major threat to ecosystems, leading to a worldwide loss of biodiversity (Tilman et al., 2017), which calls for an assessment of the conservation status of wetlands. Habitat mapping is essential to describe and monitor ecosystems because habitats result from both environmental conditions and the ecosystem's biodiversity (Lopez and Fennessy, 2002; Lu et al., 2015). Remote sensing (RS) has been identified as a pertinent source of data to derive "essential biodiversity variables", (O'Connor et al., 2015; Pereira et al., 2013), which can be used to characterize and monitor natural and semi-natural ecosystems. They also help to discriminate ecosystem distributions at the landscape scale, as well as habitat heterogeneity within these ecosystems (Alleaume et al., 2018; Skidmore et al., 2015), providing useful indicators for supporting environmental management of landscapes (Lu et al., 2015).

While habitats have been adequately mapped using RS for forest, heathland and grassland ecosystems since the early 2000s (Corbane et al., 2015), mapping inland wetlands remains challenging (Adam et al., 2010). Indeed, they encompass a wide diversity of ecosystems driven by water stress, including humid and flooded grasslands. These ecosystems are of particular interest since they provide many ecosystem services due to their hydrological, ecological and biogeochemical functionalities (Costanza et al., 1997). They provide natural and semi-natural habitats for rare fauna and flora and act as a refuge for wildlife diversity (Denny, 1994). However, human land use leads to habitat degradation (Johnston et al., 2009; Malekmohammadi and Jahanishakib, 2017), such as invasion by exotic or eutrophic indigenous species, disturbances due to intensive agriculture or development of late-successional vegetation stages due to land abandonment (Andrew and Ustin, 2009). Detecting and monitoring habitat degradation in its early stages is of major importance for land and biodiversity management (Walker and Smith, 1997). Accurately discriminating habitats and mapping wet and flooded grasslands using optical RS is challenging (Adam et al., 2010) since they exhibit high spectral and spatial variability in vegetation cover and mixtures, which can become even more confused by local properties and processes (e.g.

underlying soil, hydrological regime, atmospheric water vapor, agricultural practices). It is also difficult to define clear boundaries between habitats due to the spatio-temporal dynamics of vegetation cover caused by seasonal and annual effects of climate and human activities (Rapinel et al., 2019; Zlinszky et al., 2014). Although RS faces these challenges, it remains the only way to exhaustively map large spatial areas that could not be covered by *in-situ* surveys. Nevertheless, these surveys are crucial for training and validating RS results.

The accuracy of habitat maps depend strongly on the spectral, spatial and temporal resolutions of RS imagery. First, the use of multispectral and hyperspectral data demonstrates that as the spectral resolution increases, discrimination of habitats or species becomes easier (Adam et al., 2010). Multispectral data allow for good discrimination (Sha et al., 2008; Yang, 2007), although hyperspectral data provide more precise information about biophysical and biochemical characteristics of habitats (Erudel et al., 2017; Silvestri et al., 2003; Wang et al., 2007) or plants (Rebelo et al., 2018). However, hyperspectral data is only currently available from airborne systems, which do not provide high frequency observations over large areas except at high cost.. Second, high spatial resolution makes it possible to extract features that describe textural or multi-scale characteristics, which allows for habitat mapping at meter (Martínez-López et al., 2014) and sub-meter resolutions (Sawaya et al., 2003; Szantoi et al., 2013). Very high spatial resolution (VHSR) sensors, such as Ikonos, Quickbird or even Pleiades, however, have an associated cost that does not allow for sufficiently frequent sampling to monitor habitats continuously over large areas (Guo et al., 2017; Yang, 2007). Third, RS time series captures changes in vegetation spectra due to phenology and hydrological regimes (Wang et al., 2012; Asner, 1998). Discrimination of wetland and grassland has been improved by the use of the phenological variability in reflectance (Ouyang et al., 2013; Rapinel et al., 2019; Gilmore et al., 2008; Schuster et al., 2015). New satellite constellations such as Sentinel-2 provide high temporal frequency and spectral richness, but their spatial resolution remains too low to discriminate small or patchy habitat types effectively (Rapinel et al., 2019). Finally, no current satellite constellation offers high-frequency temporal sampling with suitable high spatial and spectral resolutions; however, optimizing the resolutions improved results (Rapinel et al., 2019). One way to

optimize resolutions is to combine several data sources, such as optical data from unmanned aerial vehicles (UAV) and satellites.

Recent technological advances have made UAVs widely available, providing a new low-cost RS data source with unrivalled properties (Anderson and Gaston, 2013). Despite their inability to cover large areas, light UAVs can acquire VHSR multispectral data (Kaneko and Nohara, 2014) at centimeter to decimeter spatial resolutions, which can be equivalent to pure pixels. They are more flexible than traditional spaceborne or airborne sensors, allowing data to be acquired at the same time as satellite data (Anderson and Gaston, 2013). Because of this flexibility, we hypothesized that UAV data can be used to complement satellite data (e.g. Pleiades, Sentinel-2) to improve mapping of wetland habitats. We assume that UAVs can play an important role between field surveys and satellite data. Indeed, automatic mapping depends on field surveys, which are expensive (Elzinga et al., 1998) and difficult to combine with satellite imagery due to spatial and temporal topological errors (Karl et al., 2014; Zhang et al., 2019) and, as mentioned, satellite resolutions that are too low. Thus, we examined whether UAVs can fill the gap between *in situ* surveys and satellites.

Our study aimed to test spectral synergies between UAV and satellite data to map plant communities, which were considered as habitat units. Reference spectra can be extracted from UAV data to map habitats at a lower spatial resolution (satellite) using a spectral unmixing approach (Roth et al., 2015). Unmixing allows the estimation of fractional abundances of distinct habitat classes that have specific spectral signatures (i.e. “endmembers”) (Keshava and Mustard, 2002). This approach has been applied to habitat mapping (Hamada et al., 2013; Silvestri et al., 2003; Wang et al., 2007) and has the advantage of considering plant communities as fuzzy sets (Bastin, 1997; Rocchini et al., 2013), due to the variation in plant abundance along soil or altitudinal gradients. The main limitation of unmixing processes is the need to select pure endmembers (or pixels), although vegetation patterns have fine-grained spatial heterogeneity. Hamada et al. (2013) pointed out that the purity of endmembers is the key to achieving good accuracy using a spectral unmixing approach. This study assumes that the spatial resolution of UAV data helps in

extracting pure endmembers.

To test these hypotheses, this study focused on the contribution of multispectral UAV data, used along with satellite data, to map habitats using three RS datasets (UAV, Sentinel-2 and Pleiades) and *in situ* floristic surveys. We focused specifically on analyzing the mosaic of habitats of a flooded grassland in France. Their temporal (time series) and spatial (textural information) resolutions were not considered.

2. Materials

2.1. Study site

The study was conducted in the Sougéal marsh (western France, 48.52° N, 1.53° W) which is part of the LTSER site “Zone Atelier Armorique”. This site is a large flooded grassland of 174 ha located in the floodplain of the Couesnon River, upstream of Mont-Saint-Michel Bay (Fig. 1). Due to its high conservation value, it has been included as a sub-site of the Natura 2000 “Baie du Mont Saint-Michel” site. It has been also labelled as a regional nature reserve. It is regularly flooded from December to April, and managed through extensive mixed-grazing of cows, horses and geese. It includes a network of shallow and stagnant channels, which enables drainage of the site in spring. Plant assemblages are driven strongly by the flooding gradient, encompassing different types of communities, from mesophilic to long-flooded communities (assemblages described in Appendix A). The corresponding habitats are identified using EUNIS typology (Ichter et al., 2014). Possible degradation of these habitats has been detected at the site, particularly the spread of competitive eutrophic plant species (e.g. *Urtica dioica*) and local trampling by cattle, which has created areas of bare soil.

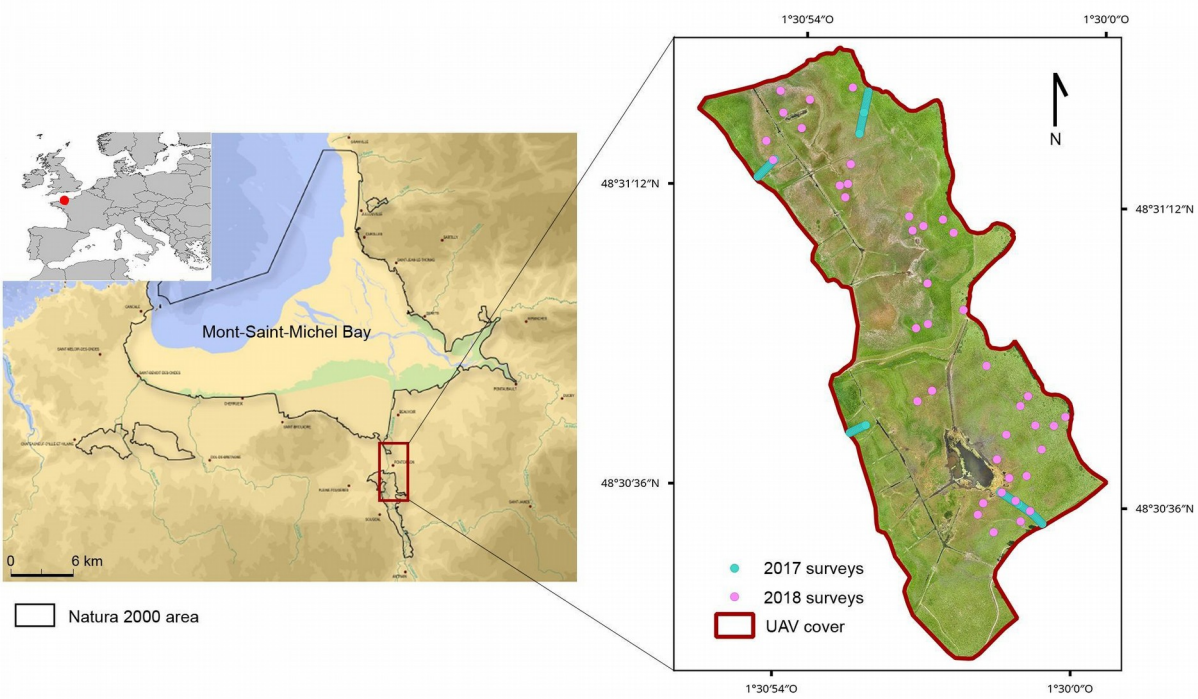


Fig. 1. (left) Location of the Sougéal marsh study site on the Mont-Saint-Michel Bay Natura 2000 site and (right) locations of floristic surveys in 2017 and 2018 on the orthophotograph acquired by UAV on 18 May 2018.

2.2. Field data

Plant assemblages were characterized by floristic surveys performed in May 2017 and May 2018 (106 and 46 sampling plots, respectively; Fig. 1). For each plot of both surveys, we recorded all plant species and estimated their abundance as a percentage of cover in the plot. The first survey was performed by distributing plots along four transects parallel to the slope of the site to survey plant communities along the gradient of flooding duration. Plots measured 2 × 2 m and were located every 5 m along the transects. The second survey was performed to supplement the first. To include all possible variants of the communities identified at the site, plots were randomly placed in spatially homogeneous areas. These plots measured 50 × 50 cm.

2.3. Remotely sensed data

2.3.1.UAV data

UAV data were acquired for three dates (6 November 2017, 20 April 2018, 18 May 2018) to

provide a multi-season dataset providing information about the phenology and seasonality of the habitats (Tomaselli et al., 2017). Two periods were selected to provide contrasting phenologies: 1) before the winter floods (i.e. in November) and 2) after the winter floods, starting in April, which corresponded to the flowering period and biomass peak, a key period for identifying floristic patterns with spectral data (Deng et al., 2017; Feilhauer et al., 2013). Although grazing had started by 18 May 2018, an exclusion zone had been established to allow vegetation to grow. Spectral responses for a given community differed depending on whether it was inside or outside this zone.

UAV data were acquired using an eBee+ (SenseFly, Cheseaux-sur-Lausanne, Switzerland), a self-guided, lightweight (1.2 kg) and fixed-wing drone. Its mean duration is 40 minutes, which allows it to cover up to 14 km² under fair meteorological conditions (low wind). Its multispectral sensor (Sequoia, Parrot SA, Paris, France) acquired 1.2 megapixel images in the green, red, red-edge and near infrared (NIR) bands (Fig. 2). It flew 148 m above the ground, providing data at a resolution of 14.7 cm, which was resampled to 20 cm to provide consistent spatial data for the study. The orthomosaics were generated for each date/spectral band using Pix4dmapper software (Pix4D SA, Lausanne, Switzerland) producing geometric error smaller than the pixel size (root mean square error (RMSE) = 0.048-0.154 m). Data were radiometrically corrected for optical instrument factors (e.g. vignetting, spectral response) and differences in solar irradiance and angle, and calibrated using a radiometric target to provide top-of-canopy (TOC) reflectance (Assmann et al., 2018).

2.3.2. Satellite data

Two types of multispectral satellite images were used: Sentinel-2 (ESA) and Pleiades (Airbus) (Table 1). Satellite data were pre-processed at level 2A (i.e. orthorectified with absolute ground reflectance values). Pleiades imaging was provided by the Centre National d'Études Spatiales (CNES, the French spatial agency) KALIDEOS program at level 1C: geometric corrections are accurate (< 0.7 m), while reflectance is retrieved using the FLAASH algorithm (Cooley et al., 2002). Sentinel-2 images were pre-processed by the CNES: radiometric corrections using the MACCS algorithm (Hagolle et al., 2015) and an

estimated positional error with an RMSE of 12.5 m (Dechoz et al., 2015) (i.e. a potential offset of > 50 pixels compared to UAV data). Pixels were adjusted empirically by shifting them to match ground-control points to minimize geometric mismatches between satellite and UAV data.

Table 1. Acquisition details for UAV, Sentinel-2 and Pleiades data.

Date	Sensor	Local time	Sensor incidence angle	Sensor azimuth angle	Solar zenith angle	Solar azimuth angle
6 Nov 2017	UAV	11:32:30	Near-nadir	/	64.181°	177.031°
6 Nov 2017	Pleiades	11:26:34	21.2762°	180.0429°	64.639°	173.643°
20 Apr 2018	UAV	11:36:30	Near-nadir	/	36.281°	170.816°
19 Apr 2018	Sentinel-2	10:56:19	Near-nadir	/	36.992°	166.341°
18 May 2018	UAV	11:10:30	Near-nadir	/	29.548°	157.664°
20 May 2018	Pleiades	11:25:34	17.7779°	180.0648°	29,298°	161.603°
19 May 2018	Sentinel-2	10:56:19	Near-nadir	/	30.369°	151.244°

Spectral characteristics of the satellite and UAV images complemented each other (Fig. 2). All satellite and UAV images were acquired under clear-sky conditions with a maximum temporal mismatch between satellite and UAV acquisition of 2 days. Consequently, we assumed that the two sets of images did not differ significantly in spectral responses.

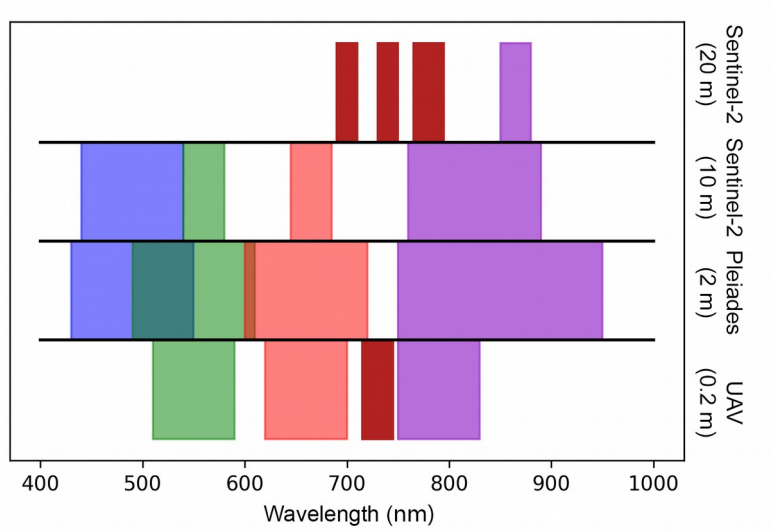


Fig. 2. Spectral (bandwidth) and spatial features of Sentinel-2, Pleiades and Sequoia (UAV) sensors.

3. Methods

The methodological workflow was stratified in four steps (Fig. 3), as described in the following subsections.

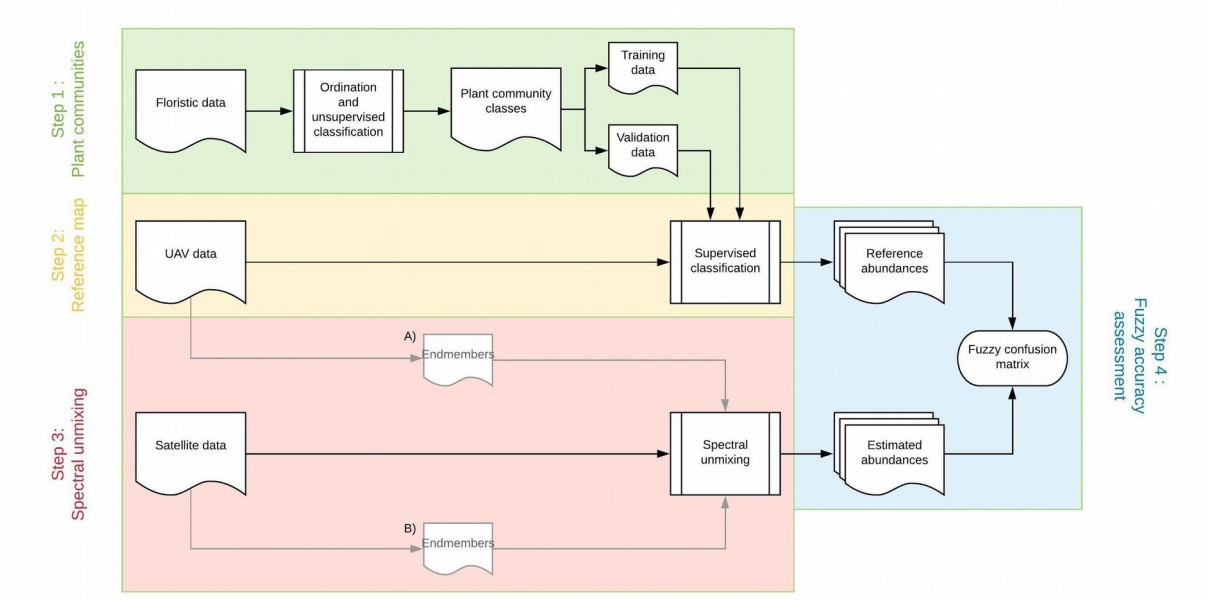


Fig. 3. The general workflow, composed of four steps: 1) unsupervised classification of floristic data, 2) supervised classification of multi-temporal UAV data to create a reference map, 3) estimation of plant community abundances by habitat based on two types of spectral unmixing (extraction of endmembers in (A) UAV imagery or (B) satellite imagery) and 4)

accuracy assessment.

3.1. Step 1: Unsupervised classification of floristic data

Plant groups were defined based on their floristic composition using correspondence analysis (Greenacre, 2010) performed using the *FactoMineR* package of R software (R Core Team, 2019). Groups were identified using hierarchical classification analysis based on the coordinates of the sampled plots on the correspondence analysis axes. Four groups were detected based on the plots sampled in 2017. Plots sampled in 2018 were projected as supplementary individuals on the multivariate plots. Each sampling plot was assigned to a group depending on its location in the multivariate plot. Seven plots that lay on the border between two groups were removed from subsequent analysis. In total, floristic groups 1-4 contained 61, 19, 39 and 26 plots, respectively.

3.2. Step 2: Reference map: supervised classification of UAV data

The spatial distribution of plant communities was mapped using a supervised classification. The entire UAV dataset, composed of spectral bands and three additional indices (NDVI, NDVI-RE and NDWI; Gitelson and Merzlyak, 1994; Rouse et al., 1974; Xie et al., 2018) from the three dates, was processed using one random forest (RF) model (Breiman, 2001). RF is an ensemble classifier that generates multiple decision trees by randomly selecting a subset of samples and variables (Belgiu and Drăguţ, 2016). It is useful for RS data because it is non-parametric and thus does not make assumptions about the distribution of the data, which are rarely Gaussian. Moreover, it provides both hard and soft classifications that correspond to probability maps of each class considered.

The RF classifier was set up to generate 300 trees. Then, the accuracy, choice of hyper-parameters and robustness of RF classification was assessed by cross validation: the sampling dataset from fields plots was divided into 10 subsets, each containing a nearly equal number of each class. Each subset served successively as learning/validation data, allowing the established model to be tested with 10 different sampling sets. The quality of the classification was assessed using the Kappa index of agreement (KIA) and the overall accuracy (OA). To optimize RF hyperparameters (maximum of features, maximum of leaf

nodes, ...), 20 values taken randomly have been tested for each subset for each subset and the best one has been kept (see Appendix B). The RF and cross validation were performed using the *scikit-learn* package in Python (Pedregosa et al., 2011).

3.3. Step 3: Estimation of abundances of plant communities

3.3.1. *State-of-the-art: A priori assumption for analyzing spectral mixtures of plant communities*

Two steps are crucial in the unmixing process: selection of endmembers and estimation of abundance. The first requires identifying the spectral signature of each endmember, which is essential because spectral unmixing is entirely dependent on - and thus sensitive to - the choice of endmembers (Tompkins et al., 1997). The flooding gradient creates fine-grained spatial variability in plant communities, which makes endmember extraction challenging. To include a wider range of variability, Multiple Endmember Spectral Mixing Analysis (MESMA) was performed, in which each endmember is represented by several spectra (Roberts et al., 1998). The second step - estimating the abundance matrix - uses the following equation (Eq. 1):

$$X = E \times A \quad \text{(Eq. 1)}$$

with X the signal received, E the endmember matrix and A the abundance matrix.

Then, MESMA attempts to minimize the residuals (Eq. 2).

$$[L(X, EA) + P(E, A)] \quad \text{(Eq. 2)}$$

with L a loss function (measuring the quality of the estimate) and P a penalty function (to force the equation to achieve desired properties).

In this study, the spectral signal was a mixture of photons that interacted with different plant species, soil and potentially water, which is assumed to be highly non-linear (Asner, 1998; Borel and Gerstl, 1994; Roberts et al., 1993).

3.3.2. SAGA+ unmixing algorithm

The unmixing algorithm used to estimate abundances was SAGA+ (Nakhostin et al., 2016),

which is based on the geometric concept of finding the simplex that embeds data. The simplex is calculated in a feature space associated with a kernel, which is useful when analyzing non-linear mixtures. Each vertex of the simplex corresponds to an endmember. Two constraints are imposed on the algorithm to avoid having all endmembers contribute to the estimated solution: 1) the sparsity level (λ), which establishes the threshold below which the abundance of an endmember becomes null, and 2) a maximum number of endmembers per pixel (n_E).

3.4. Step 4: Accuracy assessment and optimization

The accuracy of satellite unmixing was assessed by calculating a fuzzy confusion matrix, which is particularly suitable when using fuzzy classification (Binaghi et al., 1999). Unmixing can indeed be viewed as a “soft” classifier in which the proportions of classes in each pixel is extracted instead of a single class. Analyzing results with a fuzzy confusion matrix is thus more consistent than analyzing only regression between abundances, since false positives and false negatives are considered. The fuzzy confusion matrix was calculated by comparing estimated abundances to reference abundances from RF probability maps. Like hard classifications, this fuzzy matrix preserves the ability to locate errors and to derive the following indicators from soft classifications: fuzzy OA (OA_f), fuzzy KIA (KIA_f), fuzzy producer's accuracy (PA_f) and fuzzy user's accuracy (UA_f). Since the unmixing algorithm is configurable, hyperparameter optimization (Kernel sigma, λ, n_E) was performed using KIA_f as a quality criterion. The setting with the highest KIA_f was selected.

3.5. Experiments

3.5.1. Influence of acquisition features

The first experiment assessed the influence of the spatial/spectral resolutions of the satellite sensor and the acquisition period on the spectral unmixing results. In May 2018, all types of data were acquired almost simultaneously. Comparing results from Sentinel-2 and Pleiades imagery while performing the same unmixing process would allow the respective influence of the spectral and spatial resolution to be determined. The contribution of the spectral resolution of Sentinel-2 was also tested by comparing the results obtained using its full

spectral resolution to those obtained with only the spectral bands similar to those in the UAV data. Since satellite images were acquired on three dates, the influence of the state of habitats (i.e. phenology, winter flooding) during a given period could be identified. Each satellite sensor was compared among the acquisition dates. To identify the tests performed, codes were established that combined the acquisition month (nov, apr, may), satellite sensor (pl, s2) and source of endmember data (sat, uav) (Table 2).

Table 2. Codes given to the unmixing processes tested

Date	Sensor	Images used to extract endmembers	Code
6 Nov 2017	Pleiades	Pleiades	nov-pl-sat
		UAV	nov-pl-uav
20 Apr 2018	Sentinel-2	Sentinel-2	apr-s2-sat
		UAV	apr-s2-uav
18 May 2018	Sentinel-2	Sentinel-2	may-s2-sat
		UAV	may-s2-uav
	Pleiades	Pleiades	may-pl-sat
		UAV	may-pl-uav

3.5.2. *Influence of extracting endmembers from UAV vs. satellite data*

The second experiment assessed the potential of UAV data to provide suitable endmembers for unmixing habitats. Two sources of endmembers were distinguished. The classic method consisted of extracting spectra from the satellite imagery that will be processed (case B, Fig. 3). Their pixels are often assumed to be pure. The locations of sampling plots, acquired with a DGPS with a spatial accuracy of 2-3 cm, were used to extract endmembers. Since plots were separated by 5 m, however, a given pixel – especially in Sentinel-2 images (10 m spatial resolution) – may have covered two plots. If the two plots did not belong to the same habitat (i.e. the pixel covers two habitats), the corresponding spectrum was removed from the endmember matrix. Since sampling plots covered 2 × 2 m or less, even Pleiades images may have provided mixed spectral signatures, since the plots did not fit the image geometry perfectly (Fig. 4). The second method consisted of extracting endmembers from UAV images

(case A, Fig. 3), whose high spatial resolution (0.2 m) allowed us to assume that most pixels were pure (Fig. 4). Given the high spatial resolution of the UAV data, the number of spectra selected was too large to include all of them in the MESMA unmixing process; thus, the median spectral value was calculated for each sampling plot. This approach extracted endmembers of certain types and patches of vegetation that would not be detectable at lower resolutions because of their small size, such as *U. dioica* patches or bare soils, which are mainly long and narrow, corresponding to cattle pathways on the study site. The extracted endmembers are compared in Appendix C.

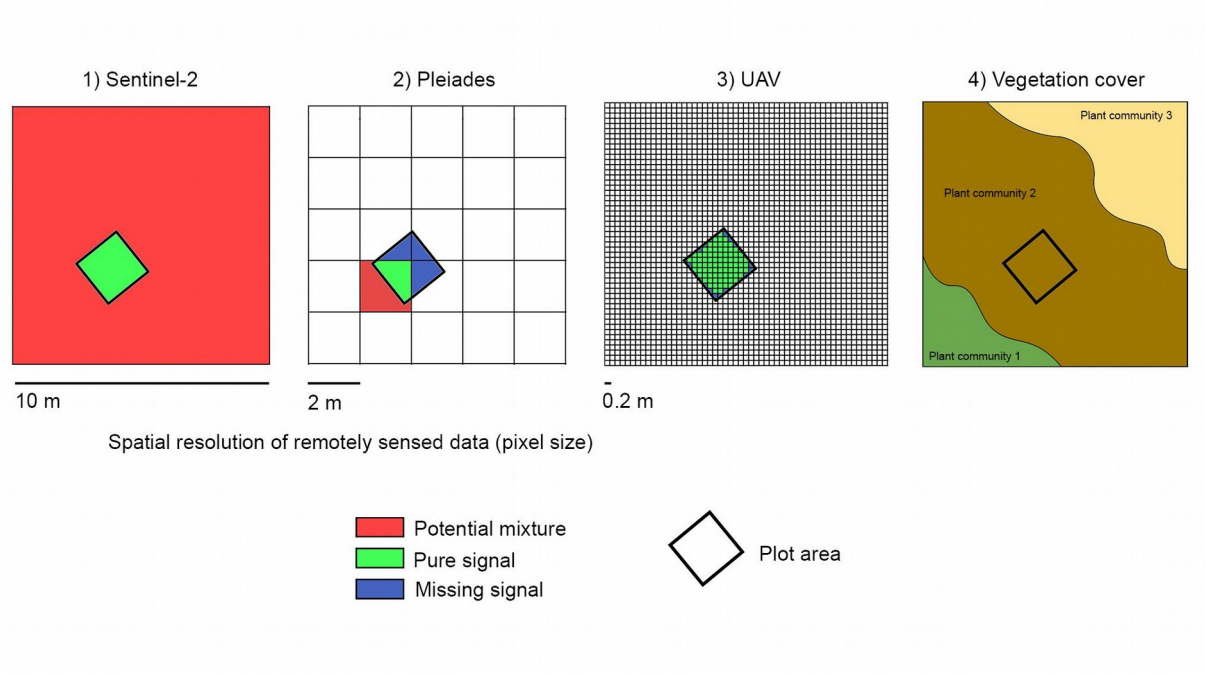


Fig. 4. Influence of spatial resolution on the spectral response of survey areas. a) Sentinel-2 resolution (10 m), b) Pleiades resolution (2 m), c) UAV resolution (0.2 m), d) Example of plant community distribution.

3.5.3. Influence of radiometric intercalibration

Combining optical RS data sources requires radiometric intercalibration. Each data source was processed for TOC reflectance. Despite these corrections, interoperability between sensors with different characteristics (e.g. spectral response, point spread function, instantaneous field of view) can produce errors (Teillet et al., 2007). To address this problem, the domain adaptation method was used (Tuia et al., 2016). This family of methods consists

of adapting data when one uses two sources with different characteristics (here, UAV and satellite data) in order to compare them effectively. In practice, UAV data are transformed to make them compatible with satellite data.

4. Results

4.1. Floristic typology

Four groups of plants were discriminated, which corresponded to plant assemblages (Appendix A) along the flooding gradient (Appendix D):

- Group 1: mesophilic (M) communities ("E2.1 Permanent mesotrophic pastures and aftermath-grazed meadows" in the EUNIS typology), dominated by *Lolium perenne*, *Poa trivialis* and *Ranunculus repens*, with *Rumex obtusifolius*, *R. crispus*, *Taraxacum officinale* and *Deschampsia cespitosa* as interstitial species.
- Groups 2 and 3: meso-hygrophilic (MH) communities ("E3.4: Moist or wet eutrophic and mesotrophic grassland" in the EUNIS typology), with group 2 dominated by *Alopecurus geniculatus and Poa trivialis*, with *Carex hirta*, *Ranunculus sardous* and *Potentilla anserine* as interstitial species; and group 3 dominated by *Eleocharis acicularis* and *Agrostis stolonifera*, with *Ranunculus flammula* as an interstitial species.
- *Group 4: hygrophilic (H) communities ("E3.4: Moist or wet eutrophic and mesotrophic grassland" in the EUNIS typology), dominated by Glyceria fluitans, with Veronica scutellata and Eleocharis palustris as interstitial species.*

4.2. Sub-pixel reference map

The supervised classification using RF and applied to multi-temporal UAV data discriminated the four plant communities with an OA of 0.83 (± 0.07) and a KIA of 0.77 (± 0.10). The two MH classes showed confusion between them (Appendix E), but once merged into a single MH class, it was discriminated well from the two others (M and H). Once merged, its classification had an OA of 0.90 (± 0.08) and a KIA of 0.85 (± 0.12). Analysis of the confusion matrix (Table 3) showed little confusion between the classes; the lowest producer's accuracy

(PA) was 0.81 for class H. Nearly all commission and omission errors were between classes M and MH or H and MH. The three other classes considered (water, bare soils and *U. dioica*) were discriminated well, with few confusions. The relative importance of features is shown in Appendix F.

Table 3. Mean confusion matrix (%) between the random forest classification of three plant communities derived from UAV imagery (columns) and sampling plots (lines). Classes: M – mesophilic; MH – meso-hygrophilic; H – hygrophilic; BS - bare soils; Ud – *Urtica dioica* and W – water. PA: Producer's accuracy, UA: User's accuracy.

		Classification							
	Class	M	MH	H	Bs	Ud	W	PA	UA
Reference	M	**31.9**	4.4	0.2				0.93	0.87
	MH	2.1	**38.8**	1.8				0.87	0.91
	H		1.5	**8.5**				0.81	0.85
	Bs				**2.8**		0.1	0.98	0.98
	Ud	0.3				**3.7**		1.00	0.92
	W						**3.9**	0.99	1.00

Plant community abundances produced by the RF model (Fig. 5) highlight the complexity of the spatial distribution of habitats and their ecotones (i.e. transitions between two habitats). Some habitats were well discriminated at the southern end of the site, while the ecotones were fuzzier at the northern end, with interlaced habitats (Fig 5a). Habitat distribution logically depended on the topography. Drier locations in highest areas corresponded to M class, and vice-versa for H class. MH class was usually located between them. At the northern end of the site, small dikes on either side of channels with MH class on them were clearly identified (Fig 5b). Comparing the distribution of RF-classified communities to field observations confirmed the accuracy of the mapping, except for one artifact: a depression in the southeast corner of the study site that contained only H class was mapped instead as a pattern of all three classes (Fig. 5c).

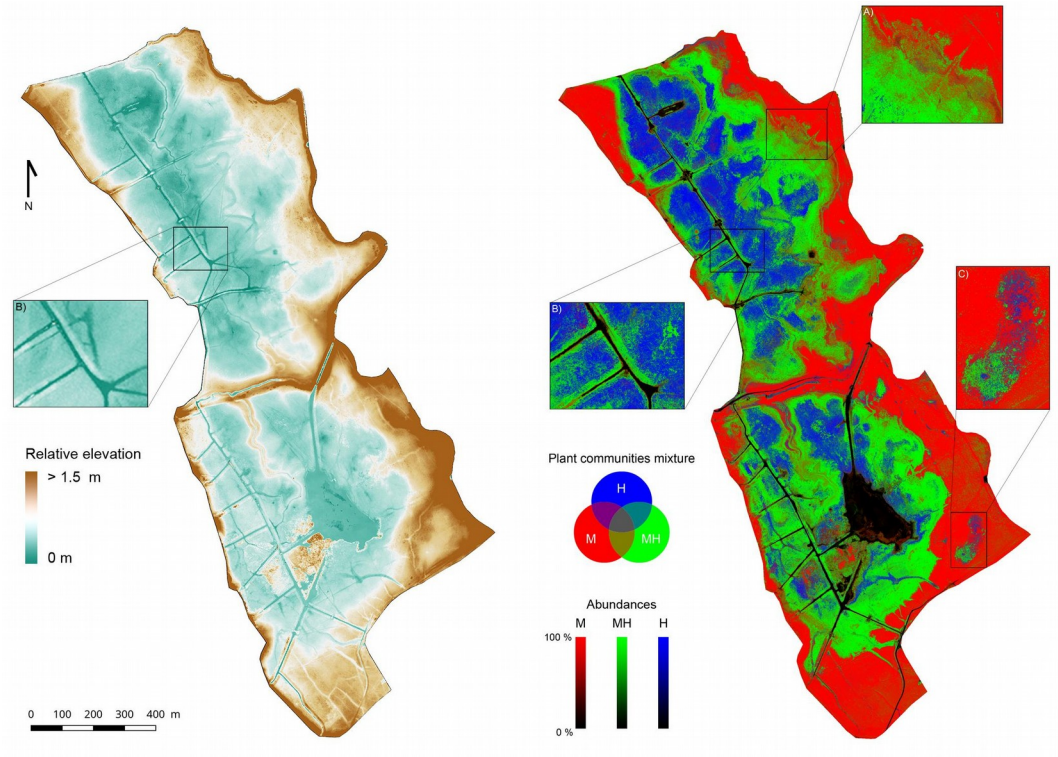


Fig. 5. Topography and plant communities of the Sougéal marsh. Left: digital surface model derived from UAV RGB data. Right: color composite of wet grassland plant communities in the Sougéal marsh derived from random forest classification of UAV imagery. Insets: a) ecotone, b) class MH on small dikes of channels and c) hygrophilic depression. Classes: M – mesophilic; MH – meso-hygrophilic; H – hygrophilic.

4.3. Abundance estimation

4.3.1. Influence of satellite acquisition features

For May 2018, the best unmixing results were obtained for may-pl-sat (OA_f = 0.68 and KIA_f = 0.53; Table 4). May-pl-sat was more effective than may-s2-sat, with a difference of +0.10 KIA_f points. The two satellite sensors identified class M well, with a UA_f and PA_f exceeding 0.70 for both (Fig. 7). However, Sentinel-2 did not detect class MH as well (PA_f = 0.40 and UA_f = 0.64) as Pleiades (PA_f = 0.63 and UA_f = 0.71). Both satellite sensors yielded poor results for bare soils, especially Sentinel-2, from whose data accurate endmembers for bare soils could not be extracted. Pleiades (Fig. 6g and 6h) clearly identified the channels, unlike Sentinel-2 (Fig. 6e and 6f). However, the latter provided higher abundances for each habitat with less plant community mixing – compared to those obtained from Pleiades (see Appendix G for details) – which is more consistent with field observations. Concerning Sentinel-2 data,

applying the same processes to a subset of satellite bands corresponding to those of the UAV yielded identical results for both acquisition dates (apr-s2-sat and may-s2-sat).

Table 4. Unmixing results by endmember sources for each Sentinel-2 and Pleiades acquisition. OA: overall accuracy, KIA: Kappa index of agreement, DA: domain adaptation.

Acquisition date	6 Nov 2017		20 Apr 2018		18 May 2018			
Sensor	Pleiades		Sentinel-2		Sentinel-2		Pleiades	
Score	OA_f	KIA_f	OA_f	KIA_f	OA_f	KIA_f	OA_f	KIA_f
Satellite endmembers	0.58	0.40	0.76	0.64	0.60	0.43	0.68	0.53
UAV endmembers	0.48	0.22	0.64	0.44	0.56	0.40	0.65	0.49
UAV endmembers (with DA)	0.58	0.38	0.71	0.57	0.65	0.51	0.65	0.51

Comparison of results highlighted the strong influence of acquisition date and solar zenith angle: scores were higher for April and lower for November. For Pleiades, scores were higher for May than for November (OA_f = 0.68 and 0.58, respectively). For Sentinel-2, scores were higher for April than for May (OA_f = 0.76 and 0.6, respectively), while Pleiades yielded a higher score than Sentinel-2 for May (OA_f = 0.65 and 0.60, respectively). Apr-s2-sat discriminated class M (PA_f = 0.80 and UA_f = 0.86) and class H class better (PA_f = 0.85 and UA_f = 0.62). Estimated abundances for November showed strong confusion between plant communities for nov-pl-sat (Fig 6a and 6b), while apr-s2-sat showed habitat patterns most similar to the reference map. Estimates for May showed clear but different patterns for classes H and MH.

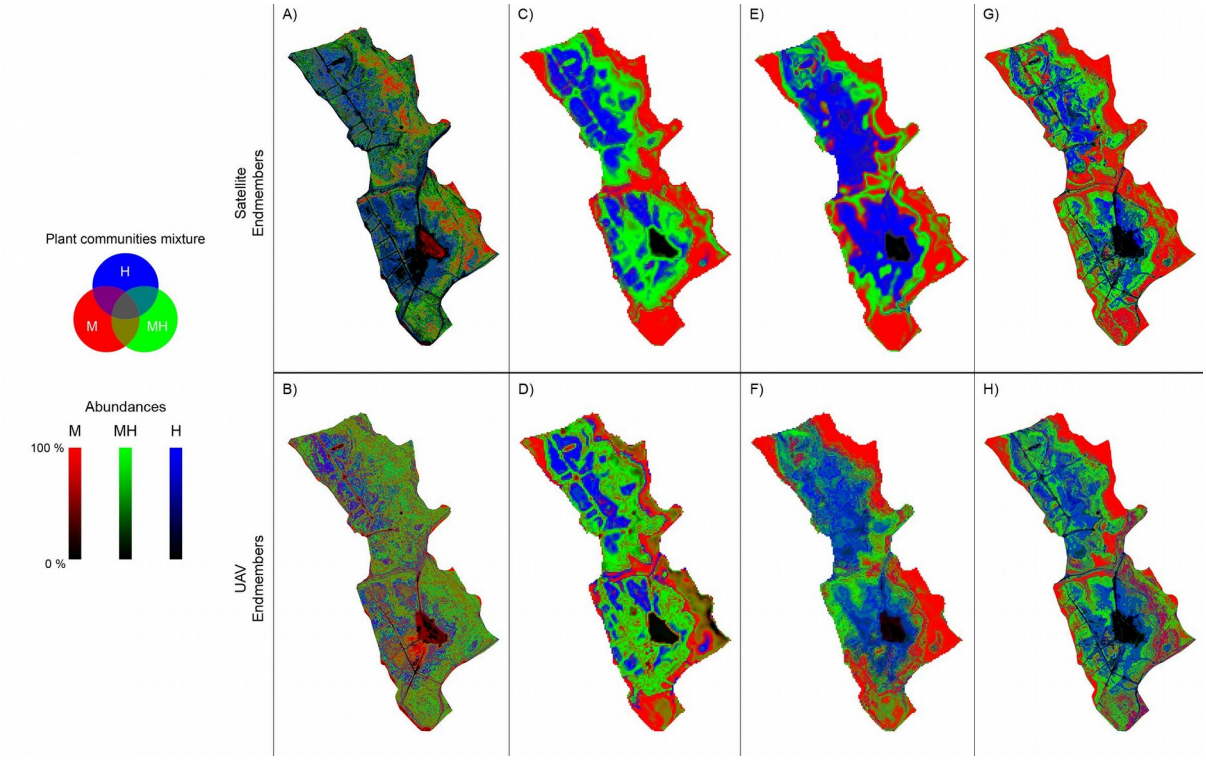


Fig. 6. Color composites of wet grassland plant communities in the Sougéal marsh derived from spectral unmixing of a) nov-pl-sat, b) nov-pl-uav, c) apr-s2-sat, d) apr-s2-uav, e) may-s2-sat, f) may-s2-uav, g) may-pl-sat, and h) may-pl-uav. See Table 2 for unmixing codes. Classes: M – mesophilic; MH – meso-hygrophilic; H – hygrophilic.

4.3.2. *Influence of endmembers extracted from UAV vs. satellite data*

UAV-extracted endmembers rarely estimated abundances better than satellite-extracted endmembers (Table 4). May-s2-uav was the only experiment in which UAV-extracted endmembers had better results than satellite-extracted endmembers (+0.08 KIA_f points compared to may-s2-sat). The other experiments showed slightly lower OA_f or KIA_f scores when using UAV endmembers. UAV endmembers did not discriminate habitat classes as clearly as satellite ones (Fig. 6, darker hues). In certain cases, however, UAV endmembers always improved the PA_f for classes that were fuzzier (MH) or covered areas often smaller than satellites' pixel size (water, bare soils) (Fig. 7). For instance, may-pl-uav endmembers estimated class MH better (i.e. higher PA_f) than Sentinel-2 or Pleiades endmembers. UAV endmembers discriminated water better, especially may-pl-uav (PA_f = 0.76 and UA_f = 0.53). For bare soils, UAV-extracted estimates were similar to those extracted from Pleiades but always better than those extracted from Sentinel-2.

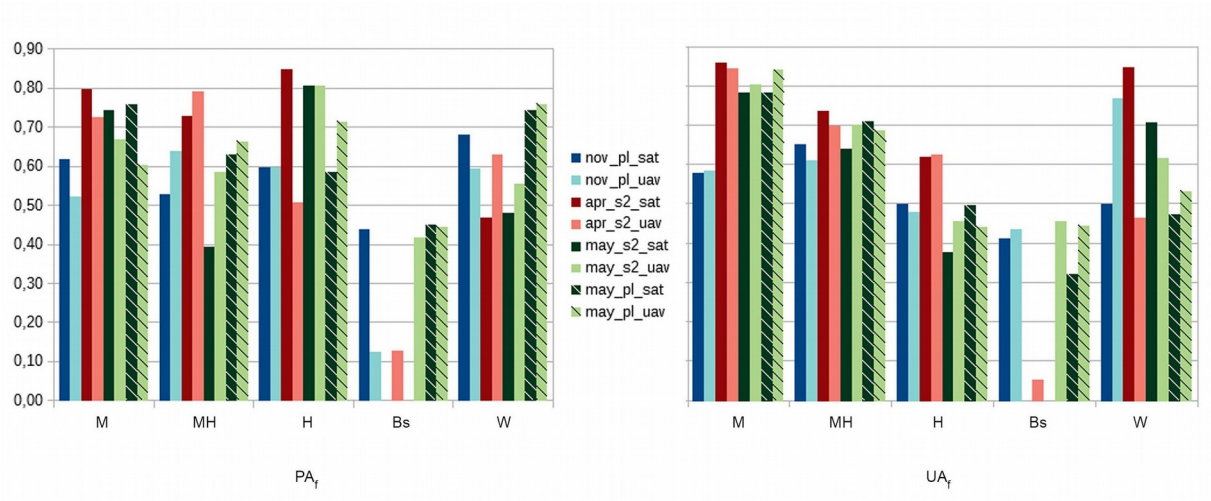
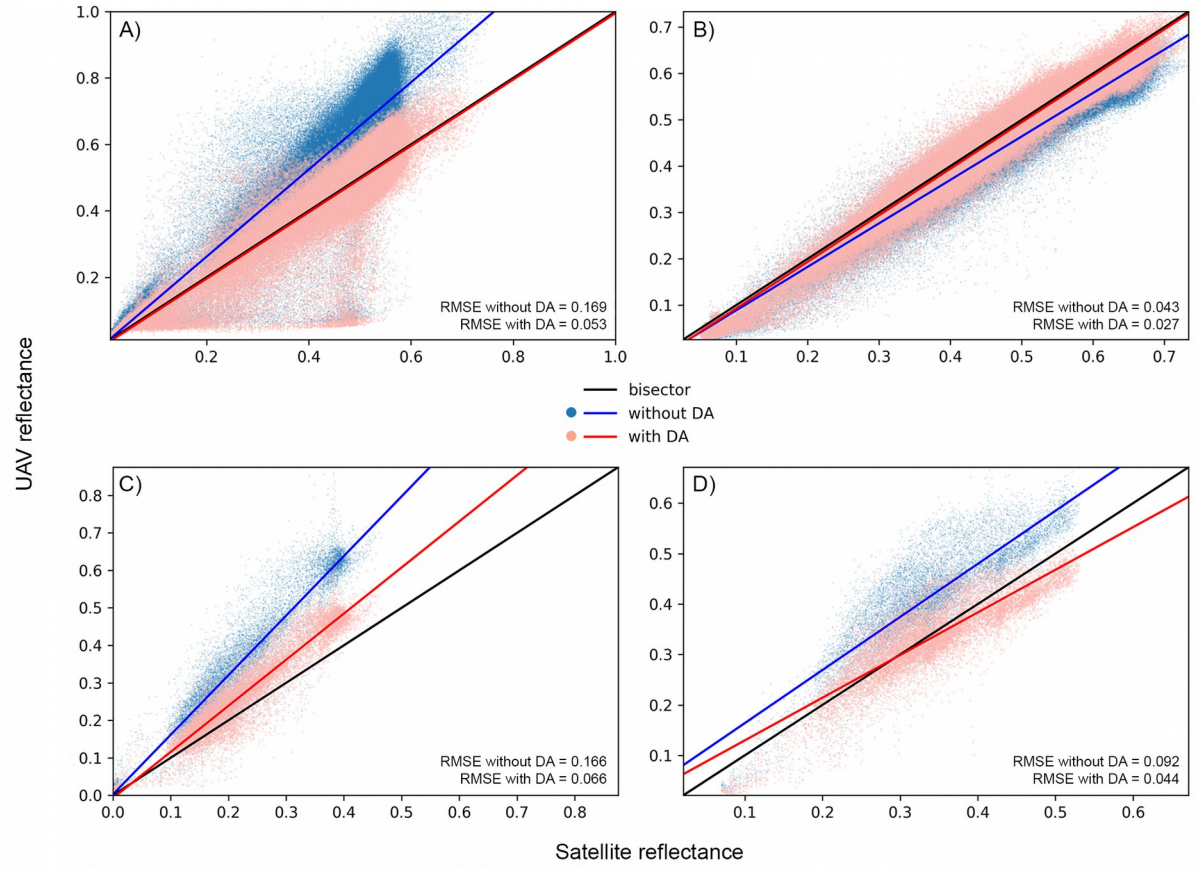


Fig. 7. Fuzzy producer's accuracy (PA_f) and user's accuracy (UA_f) by class and unmixing process. See Table 2 for unmixing codes. Classes: M – mesophilic; MH – meso-hygrophilic; H – hygrophilic; BS - bare soils; Ud – Urtica dioica and W – water.

4.3.3. Influence of radiometric intercalibration: domain adaptation

Domain adaptation adjusted the TOC reflectance values acquired with UAV to those of the satellite sensor, thus compensating for radiometric mismatches that remained after correcting each type of RS data (Fig. 8). Domain adaptation improved data intercalibration for all acquisition dates significantly: improvements were greater for November and April but less pronounced for May. Similarly, intercalibration of UAV data was better with Sentinel-2 data (Fig. 8c and 8d) than with Pleiades data (Fig. 8a and 8b).



436 Fig. 8. Scatterplots of UAV vs. satellite reflectance with (red) and without (blue) domain
437 adaptation (DA) for the near infrared spectral band: a) Pleiades on 6 November 2017, b)
438 Pleiades on 20 May 2018, c) Sentinel-2 on 19 April 2018 and d) Sentinel-2 on 19 May 2018.

439 Using domain-adapted UAV endmembers improved all unmixing results, regardless of the
440 date of acquisition (Table 5). The mean improvement was +0.09 KIA_f points, but
441 improvement varied among dates (+0.01 to +0.16 KIA_f points, +0.01 to +0.09 OA_f points).
442 The accuracy of the results was strongly correlated with the quality of the intercalibration of
443 the data sources.

444 Table 5. Improvements in spectral calibration of UAV data (RMSE) and unmixing results with
445 UAV endmembers (overall accuracy (OA_f) and Kappa index of agreement (KIA_f)) between
446 applying and not applying the domain adaptation method.

Data source and date	Δ OA_f	Δ KIA_f	Δ RMSE (NIR)
Pleiades (6 Nov 2017)	+0.09	+0.16	-0.116
Pleiades (18 May 2018)	+0.01	+0.01	-0.016

Sentinel-2 (20 Apr 2018)	+0.06	+0.09	-0.096
Sentinel-2 (19 May 2018)	+0.09	+0.11	-0.048

5. Discussion

Broadly, this study demonstrates that UAVs show great potential to fill the gap between *in situ* surveys and satellite imagery for providing and improving RS essential biodiversity variables. The spectral unmixing approach allowed for estimation of mixed habitats and overcame the spatial resolution constraint of satellite sensors by providing subpixel information. MESMA has already demonstrated its ability to integrate the variability in heterogeneous plant classes but at lower spatial resolutions (Li et al., 2005; Michishita et al., 2012; Rosso et al., 2005). When used to map natural or semi-natural habitats, it enables 1) discrimination of community patterns with a grain size smaller than the spatial resolution of the sensor (Roth et al., 2015) and 2) representation of ecotones between two habitats (Hill et al., 2007).

5.1. Endmember effectiveness in spectral, spatial and temporal dimensions

Endmember selection remains a challenging task that can be controversial. The dataset used made it possible to evaluate influences of spectral, spatial and temporal dimensions in this crucial step of habitat mapping in flooded and humid grasslands in a temperate oceanic climate.

First, spectral resolution is known to be essential for discriminating wetland plant communities (Adam et al., 2010), and it is an important feature when analyzing the spectral mixture (Bioucas-Dias et al., 2012). Surprisingly, however, we found that including all Sentinel-2 spectral bands did not improve analysis of the spectral mixture for the Sougéal marsh. The increased spectral resolution from the additional bands (6 red-edge, NIR and mid-infrared bands at 20 m) may not have compensated for the decrease in the spatial resolution. This study also shows that spectral intercalibration of RS data is crucial to perform unmixing of satellite data with endmembers from a different source. Even though data were radiometrically corrected to produce TOC reflectance, mismatches in spectral values remained between UAV and satellite data, especially in the green and NIR bands (Appendix

H). Overestimation of spectral values by the UAV‘s Sequoia multispectral sensor is suspected because its grassland reflectances exceeded 0.6 in the NIR. Domain adaptation overcame these problems, although testing the quality and interoperability of the sensor is required for future scientific studies.

Second, most endmembers extracted from high-spatial-resolution imagery yielded better results. Pleiades, with a spatial resolution 5 times as high as that of Sentinel-2, yielded better results in May 2018. One can assume that the VHSR images of Pleiades make it possible to extract endmembers that are not influenced by potential class mixtures (Roth et al., 2015). Higher-spatial-resolution UAV data can also help extract a pure spectral signature, but also one that could be too specific, depending on the grain size of plant community patterns. Nonetheless, UAV endmembers always improved discrimination of the meso-hygrophilic class, which is floristically more heterogeneous because of variations in flooding throughout the year (Bonis, 2014). This result suggests that endmembers from VHSR data are more suitable for heterogeneous classes, for which acquisition of pure pixels is more complicated. In future studies, VHSR data could be used to purify endmember spectral bands by identifying and eliminating endmembers influenced by the background (Bian et al., 2016; Ma et al., 2015).

Finally, this study strengthens the ability of RS data to discriminate plant communities better during specific periods. Like Rapinel et al. (2019), acquiring images in early spring (April), near the biomass peak and flowering of plants, appears to help discriminate plant communities greatly (Feilhauer et al., 2013). The grain size of plant community patterns may vary among periods depending on the hydrological regime (Corriale et al., 2013; Todd et al., 2010). The differences in spatial patterns identified between the periods studied (e.g. hygrophilic habitat in April and May) were likely due to confusion caused by certain species common to several habitats but not present in all vegetation belts, due to the flooding gradient over time, which causes spatial and temporal phenological shifts. Depending on land use, vegetation types and vegetation dynamics (i.e. during the acquisition period), selection of endmembers can be even more subtle than expected. Hence, integrating multi-

temporal endmembers when a phenological gradient is present is an interesting prospect (Dudley et al., 2015).

5.2. Synergies among In situ, UAV and satellite data

UAV technology shows great potential for successfully mapping habitats of the Sougéal marsh at a spatial resolution never achieved before (20 cm). VHSR imagery played two major roles in this study: clarifying and validating satellite data. First, UAV data were used to extract “pure” endmembers to clarify satellite data using the unmixing algorithm (Schaaf et al., 2011), which estimated plant community abundances. Second, combing UAV data with *in situ* surveys provided a spatially exhaustive ground truth to assess these estimated abundances. However, the accuracy of the reference map can be questioned, because spatial and temporal phenological shifts could contribute to a failure to discriminate habitats properly. For instance, ecotones can represent one of these shifts, ultimately belonging to one habitat rather than a mixture of two. Moreover, grazing activities (May-November) are likely to influence spectral signatures of plant communities and may lead to local misclassifications. Producing a monthly time series of UAV data, for instance, would help discriminate these habitats by monitoring floods and vegetation phenology.

This study focused on spectral complementarities between UAV and satellite data. Spatial and temporal complementarities still need to be explored. Indeed, UAV data provide high-resolution textural (vegetation patterns or heterogeneity) and topographical information that can be useful for habitat mapping. These spatial features can complement spectral information to differentiate complex environments in which vegetation communities have a strong spectral similarity (Zhao and Du, 2016). Object-oriented approaches that include texture information allow for multi-scale analyses (Moffett and Gorelick, 2013; Tuxen and Kelly, 2008) and could be used with a convolutional neural network to automatically extract multi-scale spatial features. This method has proven to be even more effective for wetland mapping (Mahdianpari et al., 2018; Rezaee et al., 2018) than traditional classifiers such as RF. Finally, an interesting perspective for combining UAV and satellite data is spatio-temporal fusion, which allows for modeling of high-resolution images using two data sources, one at high spatial resolution and the other at high temporal resolution (Chen et al., 2015).

5.3. Remote sensing: a proxy of the state of biodiversity

Using UAVs for RS provides good discrimination or estimation of wetland habitats at level 3 of the EUNIS typology on the Sougéal marsh, despite grazing, which prevents vegetation from developing fully. Classifying species groups into plant communities is based essentially on the presence of certain species that characterize the habitat; however, the abundances of all of its constituent species contributes most to the spectral signature of the plant community. The spectral signal acquired does not make it possible to identify the typical species of the community, which may have low abundance. On the contrary, the dominant species in the community contribute the most to the spectral signature. Nonetheless, this study demonstrates that UAV data have great potential to enhance discrimination of herbaceous habitats in humid grasslands at a fine level of nomenclature (typological resolution below EUNIS level 3), whether combined with satellite data or not.

Habitat mapping has been recognized for more than 40 years as a good proxy of biodiversity. Beyond its assessment of habitat types, this study also demonstrates that some indices of conservation status can be estimated in wetland habitats, such as the proliferation of eutrophic species (*U. dioica*) or the occurrence of local disturbances due to intensive grazing (i.e. bare soils). This opens new avenues for using UAV technology in a broader objective of analyzing the ecosystem functioning related to habitat presence, distribution and ecological status.

6. **Conclusion**

This study evaluated the utility of UAV data to fill the gap between *in situ* survey and satellite data for habitat mapping. The main results showed that UAVs have great potential for habitat mapping: they are flexible (allowing data to be acquired at the same time as satellite data), can map habitats on small areas (up to ca. 100 ha) effectively and provide training (endmember) and validation (habitat class) data for unmixing high-temporal-resolution satellite multispectral data, such as Sentinel-2 (10 m) or Pleiades (2.4 m). Fuzzy classifications of mesophilic, meso-hygrophilic and hygrophilic communities were produced with good to reasonable accuracy when combining UAV endmembers and satellite data, although the study revealed some technical limitations and the challenge of mapping of these

habitats. For the former, although it is necessary to intercalibrate sensors to increase the accuracy of habitat maps, domain adaptation can overcome spectral mismatches. For the latter, some acquisition periods were more suitable than others. The influence of climate, hydrological regimes and land use (here, grazing) may lead to spatial and temporal shifts in habitat phenology, making it difficult to discriminate boundaries of flooded grassland habitats accurately. However, UAV data contribute to early detection of invasive species or land degradation whose mean area remains smaller than the spatial resolution of satellite images. Futur work is needed to benefit fully from potential synergies between satellite and UAV data for environmental applications. Although focused only on spectral synergies, this study identified promising improvements by combining spatial and temporal characteristics.

Acknowledgements

This study was supported by public funds (Région Bretagne) received in the framework of the emerging research project (PER) coordinated by "Groupement Bretagne Télédétection" (BreTel), the ANR project MATS (ANR-18-CE23-0006) and from the European Regional Development Fund (ERDF) under the umbrella of INTERREG Atlantic Area (EAPA_261/2016) “Improving the management of Atlantic Landscapes: accounting for biodiversity and ecosystem services (ALICE)”. Data provisioning was supported by the LTSER “Zone Atelier Armorique”, the KALIDEOS Bretagne satellite acquisition program supported by the CNES and by public funds received in the framework of GEOSUD, a project (ANR-10-EQPX-20) of the "Investissements d'Avenir" program managed by the French National Research Agency and the DroneSat Project supported by the University of Rennes 2.

References

Adam, E., Mutanga, O., Rugege, D., 2010. Multispectral and hyperspectral remote sensing for identification and mapping of wetland vegetation: a review. Wetl. Ecol. Manag. 18, 281–296. https://doi.org/10.1007/s11273-009-9169-z

Alleaume, S., Dusseux, P., Thierion, V., Commagnac, L., Laventure, S., Lang, M., Féret, J.-B., Hubert-Moy, L., Luque, S., 2018. A generic remote sensing approach to derive

operational essential biodiversity variables (EBVs) for conservation planning. Methods Ecol. Evol. 9, 1822–1836. https://doi.org/10.1111/2041-210X.13033

Anderson, K., Gaston, K.J., 2013. Lightweight unmanned aerial vehicles will revolutionize spatial ecology. Front. Ecol. Environ. 11, 138–146. https://doi.org/10.1890/120150

Andrew, M.E., Ustin, S.L., 2009. Habitat suitability modelling of an invasive plant with advanced remote sensing data. Divers. Distrib. 15, 627–640. https://doi.org/10.1111/j.1472-4642.2009.00568.x

Asner, G.P., 1998. Biophysical and Biochemical Sources of Variability in Canopy Reflectance. Remote Sens. Environ. 64, 234–253. https://doi.org/10.1016/S0034-4257(98)00014-5

Assmann, J.J., Kerby, J.T., Cunliffe, A.M., Myers-Smith, I.H., 2018. Vegetation monitoring using multispectral sensors - best practices and lessons learned from high latitudes. bioRxiv 334730. https://doi.org/10.1101/334730

Bastin, L., 1997. Comparison of fuzzy c-means classification, linear mixture modelling and MLC probabilities as tools for unmixing coarse pixels. Int. J. Remote Sens. 18, 3629–3648. https://doi.org/10.1080/014311697216847

Belgiu, M., Drăguţ, L., 2016. Random forest in remote sensing: A review of applications and future directions. ISPRS J. Photogramm. Remote Sens. 114, 24–31. https://doi.org/10.1016/j.isprsjprs.2016.01.011

Bian, J., Li, A., Zhang, Z., Zhao, W., Lei, G., Xia, H., Tan, J., 2016. Grassland fractional vegetation cover monitoring using the composited HJ-1A/B time series images and unmanned aerial vehicles: A case study in Zoige wetland, China, in: 2016 IEEE International Geoscience and Remote Sensing Symposium (IGARSS). Presented at the 2016 IEEE International Geoscience and Remote Sensing Symposium (IGARSS), pp. 7192–7195. https://doi.org/10.1109/IGARSS.2016.7730876

Binaghi, E., Brivio, P.A., Ghezzi, P., Rampini, A., 1999. A fuzzy set-based accuracy assessment of soft classification. Pattern Recognit. Lett. 20, 935–948. https://doi.org/10.1016/S0167-8655(99)00061-6

Bioucas-Dias, J.M., Plaza, A., Dobigeon, N., Parente, M., Du, Q., Gader, P., Chanussot, J., 2012. Hyperspectral Unmixing Overview: Geometrical, Statistical, and Sparse Regression-Based Approaches. ArXiv12026294 Phys. Stat.

Bonis, A., 2014. Hydropériode des zones humides : un enjeu décisif pour la structure des communautés végétales et leur diversité. Lavoisier.

Borel, C.C., Gerstl, S.A.W., 1994. Nonlinear spectral mixing models for vegetative and soil surfaces. Remote Sens. Environ. 47, 403–416. https://doi.org/10.1016/0034-4257(94)90107-4

Breiman, L., 2001. Random Forests. Mach. Learn. 45, 5–32. https://doi.org/10.1023/A:1010933404324

Chen, B., Huang, B., Xu, B., 2015. Comparison of Spatiotemporal Fusion Models: A Review. Remote Sens. 7, 1798–1835. https://doi.org/10.3390/rs70201798

Cooley, T., Anderson, G.P., Felde, G.W., Hoke, M.L., Ratkowski, A.J., Chetwynd, J.H., Gardner, J.A., Adler-Golden, S.M., Matthew, M.W., Berk, A., Bernstein, L.S., Acharya, P.K., Miller, D., Lewis, P., 2002. FLAASH, a MODTRAN4-based atmospheric correction algorithm, its application and validation, in: IEEE International Geoscience and Remote Sensing Symposium. Presented at the IEEE International Geoscience and Remote Sensing Symposium, pp. 1414–1418 vol.3. https://doi.org/10.1109/IGARSS.2002.1026134

Corbane, C., Lang, S., Pipkins, K., Alleaume, S., Deshayes, M., García Millán, V.E., Strasser, T., Vanden Borre, J., Toon, S., Michael, F., 2015. Remote sensing for mapping natural habitats and their conservation status – New opportunities and challenges. Int. J. Appl. Earth Obs. Geoinformation, Special Issue on Earth observation for habitat mapping and biodiversity monitoring 37, 7–16. https://doi.org/10.1016/j.jag.2014.11.005

Corriale, M.J., Picca, P.I., di Francescantonio, D., 2013. Seasonal variation of plant communities and their environments along a topographic gradient in the Iberá wetland, ancient Paraná floodplain, Argentina. Phytocoenologia 53–69. https://doi.org/10.1127/0340-269X/2013/0043-0539

Costanza, R., d'Arge, R., Groot, R. de, Farber, S., GrasSo, M., Hannon, B., Limburg, K., Naeem, S., O'Neill, R.V., Paruelo, J., Raskin, R.G., Sutton, P., Belt, M. van den, 1997. The value of the world's ecosystem services and natural capital. Nature 387, 253. https://doi.org/10.1038/387253a0

Dechoz, C., Poulain, V., Massera, S., Languille, F., Greslou, D., de Lussy, F., Gaudel, A., L'Helguen, C., Picard, C., Trémas, T., 2015. Sentinel 2 global reference image, in: Bruzzone, L. (Ed.), . p. 96430A. https://doi.org/10.1117/12.2195046

Deng, C., Li, C., Zhu, Z., Lin, W., Xi, L., 2017. Subpixel urban impervious surface mapping: the impact of input Landsat images. ISPRS J. Photogramm. Remote Sens. 133, 89–103. https://doi.org/10.1016/j.isprsjprs.2017.09.015

Denny, P., 1994. Biodiversity and wetlands. Wetl. Ecol. Manag. 3, 55–611. https://doi.org/10.1007/BF00177296

Dudley, K.L., Dennison, P.E., Roth, K.L., Roberts, D.A., Coates, A.R., 2015. A multi-temporal spectral library approach for mapping vegetation species across spatial and temporal phenological gradients. Remote Sens. Environ., Special Issue on the Hyperspectral Infrared Imager (HyspIRI) 167, 121–134. https://doi.org/10.1016/j.rse.2015.05.004

Elzinga, C., Salzer, D., Willoughby, J., 1998. Measuring & Monitering Plant Populations. US Bur. Land Manag. Pap.

Erudel, T., Fabre, S., Houet, T., Mazier, F., Briottet, X., 2017. Criteria Comparison for Classifying Peatland Vegetation Types Using In Situ Hyperspectral Measurements. Remote Sens. 9, pages 1-62. https://doi.org/10.3390/rs9070748

Feilhauer, H., Thonfeld, F., Faude, U., He, K.S., Rocchini, D., Schmidtlein, S., 2013. Assessing floristic composition with multispectral sensors—A comparison based on monotemporal and multiseasonal field spectra. Int. J. Appl. Earth Obs. Geoinformation 21, 218–229. https://doi.org/10.1016/j.jag.2012.09.002

Gilmore, M.S., Wilson, E.H., Barrett, N., Civco, D.L., Prisloe, S., Hurd, J.D., Chadwick, C., 2008. Integrating multi-temporal spectral and structural information to map wetland vegetation in a lower Connecticut River tidal marsh. Remote Sens. Environ. 112, 4048–4060. https://doi.org/10.1016/j.rse.2008.05.020

Gitelson, A., Merzlyak, M.N., 1994. Spectral Reflectance Changes Associated with Autumn Senescence of Aesculus hippocastanum L. and Acer platanoides L. Leaves. Spectral Features and Relation to Chlorophyll Estimation. J. Plant Physiol. 143, 286–292. https://doi.org/10.1016/S0176-1617(11)81633-0

Guo, M., Li, J., Sheng, C., Xu, J., Wu, L., 2017. A Review of Wetland Remote Sensing. Sensors 17, 777. https://doi.org/10.3390/s17040777

Greenacre, M., 2010. Correspondence analysis of raw data. Ecology 91, 958–963. https://doi.org/10.1890/09-0239.1

Hagolle, O., Huc, M., Villa Pascual, D., Dedieu, G., 2015. A Multi-Temporal and Multi-Spectral Method to Estimate Aerosol Optical Thickness over Land, for the Atmospheric Correction of FormoSat-2, LandSat, VENμS and Sentinel-2 Images. Remote Sens. 7, 2668–2691. https://doi.org/10.3390/rs70302668

Hamada, Y., Stow, D.A., Roberts, D.A., Franklin, J., Kyriakidis, P.C., 2013. Assessing and monitoring semi-arid shrublands using object-based image analysis and multiple endmember spectral mixture analysis. Environ. Monit. Assess. 185, 3173–3190. https://doi.org/10.1007/s10661-012-2781-z

Hill, R.A., Granica, K., Smith, G.M., Schardt, M., 2007. Representation of an alpine treeline ecotone in SPOT 5 HRG data. Remote Sens. Environ., ForestSAT Special Issue 110, 458–467. https://doi.org/10.1016/j.rse.2006.11.031

Ichter, J., Evans, D., Richard, D., Poncet, L., Spyropoulou, R., Pereira Martins, I., European Environment Agency, Museum national d'Histoire naturelle (MNHN), 2014. Terrestrial habitat mapping in Europe: an overview. Publications Office, Luxembourg.

Johnston, C.A., Zedler, J.B., Tulbure, M.G., Frieswyk, C.B., Bedford, B.L., Vaccaro, L., 2009. A unifying approach for evaluating the condition of wetland plant communities and identifying related stressors. Ecol. Appl. 19, 1739–1757. https://doi.org/10.1890/08-1290.1

Karl, J.W., Taylor, J., Bobo, M., 2014. A double-sampling approach to deriving training and validation data for remotely-sensed vegetation products. Int. J. Remote Sens. 35, 1936–1955. https://doi.org/10.1080/01431161.2014.880820Kaneko, K., Nohara, S.,

2014. Review of Effective Vegetation Mapping Using the UAV (Unmanned Aerial Vehicle) Method. J. Geogr. Inf. Syst. 06, 733–742. https://doi.org/10.4236/jgis.2014.66060

Keshava, N., Mustard, J.F., 2002. Spectral unmixing. IEEE Signal Process. Mag. 19, 44–57. https://doi.org/10.1109/79.974727

Li, L., Ustin, S.L., Lay, M., 2005. Application of multiple endmember spectral mixture analysis (MESMA) to AVIRIS imagery for coastal salt marsh mapping: a case study in China Camp, CA, USA. Int. J. Remote Sens. 26, 5193–5207. https://doi.org/10.1080/01431160500218911

Lopez, R.D., Fennessy, M.S., 2002. Testing the Floristic Quality Assessment Index as an Indicator of Wetland Condition. Ecol. Appl. 12, 487–497. https://doi.org/10.1890/1051-0761(2002)012[0487:TTFQAI]2.0.CO;2

Lu, Y., Wang, R., Zhang, Y., Su, H., Wang, P., Jenkins, A., Ferrier, R.C., Bailey, M., Squire, G., 2015. Ecosystem health towards sustainability. Ecosyst. Health Sustain. 1, 1–15. https://doi.org/10.1890/EHS14-0013.1

Ma, L., Zhou, Y., Chen, J., Cao, X., Chen, X., 2015. Estimation of Fractional Vegetation Cover in Semiarid Areas by Integrating Endmember Reflectance Purification Into Nonlinear Spectral Mixture Analysis. IEEE Geosci. Remote Sens. Lett. 12, 1175–1179. https://doi.org/10.1109/LGRS.2014.2385816

Mahdianpari, M., Salehi, B., Rezaee, M., Mohammadimanesh, F., Zhang, Y., 2018. Very Deep Convolutional Neural Networks for Complex Land Cover Mapping Using Multispectral Remote Sensing Imagery. Remote Sens. 10, 1119. https://doi.org/10.3390/rs10071119

Malekmohammadi, B., Jahanishakib, F., 2017. Vulnerability assessment of wetland landscape ecosystem services using driver-pressure-state-impact-response (DPSIR) model. Ecol. Indic. 82, 293–303. https://doi.org/10.1016/j.ecolind.2017.06.060

Martínez-López, J., Carreño, M.F., Palazón-Ferrando, J.A., Martínez-Fernández, J., Esteve, M.A., 2014. Remote sensing of plant communities as a tool for assessing the condition of semiarid Mediterranean saline wetlands in agricultural catchments. Int. J.

Appl. Earth Obs. Geoinformation 26, 193–204. https://doi.org/10.1016/j.jag.2013.07.005

Michishita, R., Gong, P., Xu, B., 2012. Spectral mixture analysis for bi-sensor wetland mapping using Landsat TM and Terra MODIS data. Int. J. Remote Sens. 33, 3373–3401. https://doi.org/10.1080/01431161.2011.611185

Moffett, K.B., Gorelick, S.M., 2013. Distinguishing wetland vegetation and channel features with object-based image segmentation. Int. J. Remote Sens. 34, 1332–1354. https://doi.org/10.1080/01431161.2012.718463

Nakhostin, S., Clenet, H., Corpetti, T., Courty, N., 2016. Joint Anomaly Detection and Spectral Unmixing for Planetary Hyperspectral Images. IEEE Trans. Geosci. Remote Sens. 54, 6879–6894. https://doi.org/10.1109/TGRS.2016.2586188

O'Connor, B., Secades, C., Penner, J., Sonnenschein, R., Skidmore, A., Burgess, N.D., Hutton, J.M., 2015. Earth observation as a tool for tracking progress towards the Aichi Biodiversity Targets. Remote Sens. Ecol. Conserv. 1, 19–28. https://doi.org/10.1002/rse2.4

Ouyang, Z.-T., Gao, Y., Xie, X., Guo, H.-Q., Zhang, T.-T., Zhao, B., 2013. Spectral Discrimination of the Invasive Plant Spartina alterniflora at Multiple Phenological Stages in a Saltmarsh Wetland. PloS One 8, e67315. https://doi.org/10.1371/journal.pone.0067315

Pedregosa, F., Varoquaux, G., Gramfort, A., Michel, V., Thirion, B., Grisel, O., Blondel, M., Prettenhofer, P., Weiss, R., Dubourg, V., Vanderplas, J., Passos, A., Cournapeau, D., Brucher, M., Perrot, M., Duchesnay, É., 2011. Scikit-learn: Machine Learning in Python. J. Mach. Learn. Res. 12, 2825–2830.

Pereira, H.M., Ferrier, S., Walters, M., Geller, G.N., Jongman, R.H.G., Scholes, R.J., Bruford, M.W., Brummitt, N., Butchart, S.H.M., CardoSo, A.C., Coops, N.C., Dulloo, E., Faith, D.P., Freyhof, J., Gregory, R.D., Heip, C., Höft, R., Hurtt, G., Jetz, W., Karp, D.S., McGeoch, M.A., Obura, D., Onoda, Y., Pettorelli, N., Reyers, B., Sayre, R., Scharlemann, J.P.W., Stuart, S.N., Turak, E., Walpole, M., Wegmann, M., 2013.

760 Essential Biodiversity Variables. Science 339, 277–278.
761 https://doi.org/10.1126/science.1229931
762 Pix4D. 2019. Support website. Available from https://support.pix4d.com/hc/en-us [accessed
763 18 October 2019]
764 Rapinel, S., Mony, C., Lecoq, L., Clément, B., Thomas, A., Hubert-Moy, L., 2019. Evaluation
765 of Sentinel-2 time-series for mapping floodplain grassland plant communities. Remote
766 Sens. Environ. 223, 115–129. https://doi.org/10.1016/j.rse.2019.01.018
767 Rebelo, A.J., Somers, B., Esler, K.J., Meire, P., 2018. Can wetland plant functional groups
768 be spectrally discriminated? Remote Sens. Environ. 210, 25–34.
769 https://doi.org/10.1016/j.rse.2018.02.031
770 Rezaee, M., Mahdianpari, M., Zhang, Y., Salehi, B., 2018. Deep Convolutional Neural
771 Network for Complex Wetland Classification Using Optical Remote Sensing Imagery.
772 IEEE J. Sel. Top. Appl. Earth Obs. Remote Sens. 11, 3030–3039.
773 https://doi.org/10.1109/JSTARS.2018.2846178
Roberts, D.A., Smith, M.O., Adams, J.B., 1993. Green vegetation, nonphotosynthetic
vegetation, and soils in AVIRIS data. Remote Sens. Environ., Airbone Imaging
Spectrometry 44, 255–269. https://doi.org/10.1016/0034-4257(93)90020-X
774 Roberts, D.A., Gardner, M., Church, R., Ustin, S., Scheer, G., Green, R.O., 1998. Mapping
775 Chaparral in the Santa Monica Mountains Using Multiple Endmember Spectral
776 Mixture Models. Remote Sens. Environ. 65, 267–279. https://doi.org/10.1016/S0034-
777 4257(98)00037-6
778 Rocchini, D., Foody, G.M., Nagendra, H., Ricotta, C., Anand, M., He, K.S., Amici, V.,
779 Kleinschmit, B., Förster, M., Schmidtlein, S., Feilhauer, H., Ghisla, A., Metz, M.,
780 Neteler, M., 2013. Uncertainty in ecosystem mapping by remote sensing. Comput.
781 Geosci., Benchmark problems, datasets and methodologies for the computational
782 geosciences 50, 128–135. https://doi.org/10.1016/j.cageo.2012.05.022
783 Rosso, P.H., Ustin, S.L., Hastings, A., 2005. Mapping marshland vegetation of San
784 Francisco Bay, California, using hyperspectral data. Int. J. Remote Sens. 26, 5169–
785 5191. https://doi.org/10.1080/01431160500218770

Roth, K.L., Roberts, D.A., Dennison, P.E., Peterson, S.H., Alonzo, M., 2015. The impact of spatial resolution on the classification of plant species and functional types within imaging spectrometer data. Remote Sens. Environ. 171, 45–57. https://doi.org/10.1016/j.rse.2015.10.004

Rouse, J.W., Jr., Haas, R.H., Schell, J.A., Deering, D.W., 1974. Monitoring Vegetation Systems in the Great Plains with Erts. NASA Spec. Publ. 351, 309.

Sawaya, K.E., Olmanson, L.G., Heinert, N.J., Brezonik, P.L., Bauer, M.E., 2003. Extending satellite remote sensing to local scales: land and water resource monitoring using high-resolution imagery. Remote Sens. Environ., IKONOS Fine Spatial Resolution Land Observation 88, 144–156. https://doi.org/10.1016/j.rse.2003.04.006

Schaaf, A.N., Dennison, P.E., Fryer, G.K., Roth, K.L., Roberts, D.A., 2011. Mapping Plant Functional Types at Multiple Spatial Resolutions Using Imaging Spectrometer Data. GIScience Remote Sens. 48, 324–344. https://doi.org/10.2747/1548-1603.48.3.324

Schuster, C., Schmidt, T., Conrad, C., Kleinschmit, B., Förster, M., 2015. Grassland habitat mapping by intra-annual time series analysis – Comparison of RapidEye and TerraSAR-X satellite data. Int. J. Appl. Earth Obs. Geoinformation 34, 25–34. https://doi.org/10.1016/j.jag.2014.06.004

Sha, Z., Bai, Y., Xie, Y., Yu, M., Zhang, L., 2008. Using a hybrid fuzzy classifier (HFC) to map typical grassland vegetation in Xilin River Basin, Inner Mongolia, China. Int. J. Remote Sens. 29, 2317–2337. https://doi.org/10.1080/01431160701408436

Silvestri, S., Marani, M., Marani, A., 2003. Hyperspectral remote sensing of salt marsh vegetation, morphology and soil topography. Phys. Chem. Earth Parts ABC, Applications of Quantitative Remote Sensing to Hydrology 28, 15–25. https://doi.org/10.1016/S1474-7065(03)00004-4

Skidmore, A.K., Pettorelli, N., Coops, N.C., Geller, G.N., Hansen, M., Lucas, R., Mücher, C.A., O'Connor, B., Paganini, M., Pereira, H.M., Schaepman, M.E., Turner, W., Wang, T., Wegmann, M., 2015. Environmental science: Agree on biodiversity metrics to track from space. Nat. News 523, 403. https://doi.org/10.1038/523403a

814 Szantoi, Z., Escobedo, F., Abd-Elrahman, A., Smith, S., Pearlstine, L., 2013. Analyzing fine-
815 scale wetland composition using high resolution imagery and texture features. Int. J.
816 Appl. Earth Obs. Geoinformation 23, 204–212.
817 https://doi.org/10.1016/j.jag.2013.01.003
818 Teillet, P.M., Fedosejevs, G., Thome, K.J., Barker, J.L., 2007. Impacts of spectral band
819 difference effects on radiometric cross-calibration between satellite sensors in the
820 solar-reflective spectral domain. Remote Sens. Environ. 110, 393–409.
821 https://doi.org/10.1016/j.rse.2007.03.003
822 Tilman, D., Clark, M., Williams, D.R., Kimmel, K., Polasky, S., Packer, C., 2017. Future
823 threats to biodiversity and pathways to their prevention. Nature 546, 73.
824 https://doi.org/10.1038/nature22900
825 Todd, M.J., Muneepeerakul, R., Pumo, D., Azaele, S., Miralles-Wilhelm, F., Rinaldo, A.,
826 Rodriguez-Iturbe, I., 2010. Hydrological drivers of wetland vegetation community
827 distribution within Everglades National Park, Florida. Adv. Water Resour., Special
828 Issue on Novel Insights in Hydrological Modelling 33, 1279–1289.
829 https://doi.org/10.1016/j.advwatres.2010.04.003
830 Tomaselli, V., Adamo, M., Veronico, G., Sciandrello, S., Tarantino, C., Dimopoulos, P.,
831 Medagli, P., Nagendra, H., Blonda, P., 2017. Definition and application of expert
832 knowledge on vegetation pattern, phenology, and seasonality for habitat mapping, as
833 exemplified in a Mediterranean coastal site. Plant Biosyst. - Int. J. Deal. Asp. Plant
834 Biol. 151, 887–899. https://doi.org/10.1080/11263504.2016.1231143
835 Tompkins, S., Mustard, J.F., Pieters, C.M., Forsyth, D.W., 1997. Optimization of
836 endmembers for spectral mixture analysis. Remote Sens. Environ. 59, 472–489.
837 https://doi.org/10.1016/S0034-4257(96)00122-8
838 Tuia, D., Persello, C., Bruzzone, L., 2016. Domain adaptation for the classification of remote
839 sensing data: an overview of recent advances. IEEE Geosci. Remote Sens. Mag. 4,
840 41–57. https://doi.org/10.1109/MGRS.2016.2548504
841 Tuxen, K., Kelly, M., 2008. Multi-scale functional mapping of tidal marsh vegetation using
842 object-based image analysis, in: Blaschke, T., Lang, S., Hay, G.J. (Eds.), Object-

Based Image Analysis: Spatial Concepts for Knowledge-Driven Remote Sensing Applications, Lecture Notes in Geoinformation and Cartography. Springer Berlin Heidelberg, Berlin, Heidelberg, pp. 415–442. https://doi.org/10.1007/978-3-540-77058-9_23

Walker, L.R., Smith, S.D., 1997. Impacts of Invasive Plants on Community and Ecosystem Properties, in: Luken, J.O., Thieret, J.W. (Eds.), Assessment and Management of Plant Invasions, Springer Series on Environmental Management. Springer New York, New York, NY, pp. 69–86. https://doi.org/10.1007/978-1-4612-1926-2_7

Wang, C., Menenti, M., Stoll, M.-P., Belluco, E., Marani, M., 2007. Mapping mixed vegetation communities in salt marshes using airborne spectral data. Remote Sens. Environ. 107, 559–570. https://doi.org/10.1016/j.rse.2006.10.007

Wang, L., Dronova, I., Gong, P., Yang, W., Li, Y., Liu, Q., 2012. A new time series vegetation–water index of phenological–hydrological trait across species and functional types for Poyang Lake wetland ecosystem. Remote Sens. Environ. 125, 49–63. https://doi.org/10.1016/j.rse.2012.07.003

Xie, Q., Dash, J., Huang, W., Peng, D., Qin, Q., Mortimer, H., Casa, R., Pignatti, S., Laneve, G., Pascucci, S., Dong, Y., Ye, H., 2018. Vegetation Indices Combining the Red and Red-Edge Spectral Information for Leaf Area Index Retrieval. IEEE J. Sel. Top. Appl. Earth Obs. Remote Sens. 11, 1482–1493. https://doi.org/10.1109/JSTARS.2018.2813281

Yang, X., 2007. Integrated use of remote sensing and geographic information systems in riparian vegetation delineation and mapping. Int. J. Remote Sens. 28, 353–370. https://doi.org/10.1080/01431160600726763

Zhang, J., Okin, G.S., Zhou, B., 2019. Assimilating optical satellite remote sensing images and field data to predict surface indicators in the Western U.S.: Assessing error in satellite predictions based on large geographical datasets with the use of machine learning. Remote Sens. Environ. 233, 111382. https://doi.org/10.1016/j.rse.2019.111382

871 Zhao, W., Du, S., 2016. Learning multiscale and deep representations for classifying
872 remotely sensed imagery. ISPRS J. Photogramm. Remote Sens. 113, 155–165.
873 https://doi.org/10.1016/j.isprsjprs.2016.01.004
874 Zlinszky, A., Schroiff, A., Kania, A., Deák, B., Mücke, W., Vári, Á., Székely, B., Pfeifer, N.,
875 2014. Categorizing Grassland Vegetation with Full-Waveform Airborne Laser
876 Scanning: A Feasibility Study for Detecting Natura 2000 Habitat Types. Remote
877 Sens. 6, 8056–8087. https://doi.org/10.3390/rs6098056

878
879 **Figure captions**

880 Fig. 1: (left) Location of the Sougéal marsh study site on the Mont-Saint-Michel Bay Natura
881 2000 site and (right) locations of floristic surveys in 2017 and 2018 on the orthophotograph
882 acquired by UAV on 18 May 2018.

883 Fig. 2: Spectral (band width) and spatial features of Sentinel-2, Pleiades and Sequoia (UAV)
884 sensors.

885 Fig. 3: The general processing workflow composed by four steps. 1) Unsupervised
886 classification of floristic data. 2) Supervised classification of multidate UAV data to provide a
887 reference map. 3) Estimation of habitats' abundances using spectral unmixing with two
888 cases: A) extraction of endmembers in UAV imagery; and B) extraction of endmembers in
889 satellite imagery. 4) accuracy assessment.

890 Fig. 4: Impact of spatial resolution on the spectral response of survey areas. a) Sentinel-2
891 resolution (10m) ; b) Pleiades resolution (2m) ; c) UAV resolution (0.2m) ; d) Example of
892 plant communities distribution.

893 Fig. 5: Topography and plant communities of the Sougeal marsh. Left: digital surface model
894 derived from UAV RGB data. Right: color composite of wet grasslands plant communities in
895 the Sougeal marsh derived from RF classification of UAV imagery. Specific areas: a)
896 ecotone; b) MH on small dikes of channels; c) hygrophilic depression. Classes description: M
897 – Mesophilic; MH – Meso-Hygrophilic; H – Hygrophilic.

898 Fig. 6: Color composites of wet grasslands plant communities in the Sougeal marsh derived
899 from spectral unmixing of a) nov-pl-sat, b) nov-pl-uav, c) apr-s2-sat, d) apr-s2-uav, e) may-
900 s2-sat, f) may-s2-uav, g) may-pl-sat, and h) may-pl-uav. Classes description: M – Mesophilic;
901 MH – Meso-Hygrophilic; H – Hygrophilic.

902 Fig. 7: Fuzzy producer's (PA_f) and user's (UA_f) accuracy per classes and unmixing
903 processes. Classes description: M – Mesophilic; MH – Meso-Hygrophilic; H – Hygrophilic; BS
904 - Bare soils; Ud – Urtica dioica and W – Water. PA: Producer's accuracy, UA: User's

905 accuracy.

906 Fig. 8: Scatter plots of UAV versus Satellite measurements with (red) and without (blue) DA
907 for the NIR spectral band: a) Pleiades at 2017-11-06; b) Pleiades at 2018-05-20; c) Sentinel-
908 2 at 2018-04-19 ; and d) Sentinel-2 at 2018-05-19.